International Journal of Fatigue 64 (2014) 84–96

Contents lists available at ScienceDirect

International Journal of Fatigue

journal homepage: www.elsevier.com/locate/ijfatigue

Degradation of titanium 6Al–4V fatigue strength due to electrical discharge machining

Todd M. Mower *

M.I.T. Lincoln Laboratory, 244 Wood Street, Lexington, MA 02420, United States

ARTICLE INFO

Article history:
Received 5 April 2013
Received in revised form 9 January 2014
Accepted 23 February 2014
Available online 6 March 2014

Keywords:
Fatigue strength degradation
Electrical discharge machining (EDM)
Ti–6Al–4V
Recast layer
Surface roughness

ABSTRACT

Electrical discharge machining (EDM) has been known for many years to induce degradation of fatigue strength. Outdated or coarse EDM processing methods can reduce the fatigue strength of titanium alloy Ti–6Al–4V by as much as factors of 2–5, but a paucity of fatigue data exists for this important aerospace alloy processed with modern EDM techniques. An experimental study is presented in which the degradation of fatigue strength of Ti–6Al–4V due to improved EDM processing is measured in axial tension at a load ratio of $R = 0.1$. It is shown that, relative to specimens finely milled, state-of-the-art EDM processing causes a reduction of fatigue strength by 15–30%. This strength degradation is found to correlate directly to the thickness and roughness of recast layers created by the solidification of melt material formed during EDM. Post-processing with either electrochemical polishing or bead blasting is demonstrated to remove the deleterious effects of EDM, such that specimens possessed intrinsic fatigue behavior as indicated by crack initiation at interior locations.

1. Introduction

1.1. Background

Of all the titanium alloys that have been developed, the dual-phase ($\alpha + \beta$) alloy Ti–6Al–4V is the most commonly utilized, accounting for more than 50% of the titanium components presently in use [1]. Applications of Ti–6Al–4V can be found throughout the aerospace industry, ranging from large (>1 m) first-stage compressor fans in gas turbines to small (~1 cm) flexures used to support sensitive instruments on space payloads. To enable efficient design of these components subject to large cyclic stresses, engineers need fatigue data generated with test specimens fabricated using relevant methods. An increasingly important method is electrical discharge machining (EDM), which enables precise, rapid and repeatable machining of metals.

The effect upon high-cycle fatigue behavior of various machining techniques used on annealed titanium alloy Ti–6Al–4V is presented in a bar chart published in *Titanium, a Technical Guide* [2]; that chart shows the fatigue limit ranging from 441 to 503 MPa for components fabricated with conventional milling and turning techniques. Machining with EDM is represented as reducing the fatigue limit to only 166 MPa. These data were published previously in a journal article [3] that provided no information regarding the testing procedures used or surface condition of the specimens tested.

During the three decades that have passed since the generation of the data cited above, many improvements have been implemented in EDM equipment technology and processing parameters. Modern EDM operations are capable of producing finished cuts with much smoother surfaces and thinner "recast layers" than were possible with older techniques. Because EDM surface layers typically experience residual tensile stress and are often populated with many microcracks, reduction of these compromising factors is anticipated to result in improved fatigue strength/life relative to that achieved with former EDM methods. Despite the advances in EDM technologies that are allowing engineers to fabricate more intricate components (which are often subjected to increasingly higher cyclic stresses), very little quantitative data appear to exist in the published literature regarding the degradation of fatigue behavior caused by contemporary EDM processing of titanium alloys.

1.2. Brief review of related investigations

The fatigue data used most widely for the purpose of designing aerospace components fabricated from titanium alloys have been compiled as stress–lifetime (S–N) plots in the Military Handbook 5, first published in 1959 and most recently revised in 2003. (This

* Tel.: +1 (781) 981 3533.
E-mail address: mower@ll.mit.edu

http://dx.doi.org/10.1016/j.ijfatigue.2014.02.018
0142-1123/

document has been superseded by the Metallic Materials Properties Development & Standardization, MMPDS.) Seven such plots are included for Ti–6Al–4V, providing data from axial fatigue tests using specimens machined conventionally (meaning with rotating milling tools, grinding and/or mechanical polishing) and subjected to various, listed testing parameters [4]. A common trait among all these data is the extreme range of scatter: for nearly every set of specimens and test conditions, the measured lifetimes at a given level of stress ranged by at least two and sometimes three orders of magnitude. Alternatively, quite similar lifetimes are demonstrated by cyclic stresses differing by 20–30%.

Very recent research with conventionally-machined $\alpha + \beta$ Ti–6Al–4V has focused upon experimental investigation of the intrinsic cause of variability in measured fatigue strengths. Tensile fatigue tests were conducted with specimens that were machined in a lathe, ground with "low stress" and mechanically polished; a subgroup of specimens were also electropolished. The results demonstrated lifetimes varying by more than an order of magnitude, at a given level of stress, and suggested that a "short-life" mode of fatigue crack initiation evolving at near-surface alpha grains was suppressed by the grinding process [5]. In further development of this work, it was shown that grain-facet formation and orientation influenced strongly whether fatigue cracks in this dual-phase alloy proceeded along a short or long-life trajectory [6]. These studies suggest that a significant, and possibly major, portion of the scatter observed in Ti–6Al–4V fatigue data can be due solely to aspects of metallurgy. Although fatigue-life variability is not the focus of the research presented herein, it is important to bear in mind since it has the potential to cause misinterpretation of fatigue data generated with dual-phase Ti–6Al–4V alloys.

One of the earliest published, quantitative indications of the effect of EDM on fatigue strength of titanium appears in the (1974) *Military Handbook on Titanium and Titanium Alloys* [7]. Fig. 12 of the *Handbook* portrays the effect of machining technique on fully reversed (rotating beam) fatigue life of Ti–5Al–2.5Sn. The plot indicates the fatigue strength for 10^6 cycles is reduced from approximately 428 MPa for "as rolled", to about 212 MPa for EDM processed specimens. Only trendlines are presented however, not discrete data, and no details were provided concerning specimen preparation and surface roughness or material condition.

Experimental investigations of the influence on fatigue strength of EDM processing of tool steels were published in 2001. Rotating-beam tests with D2 tool-steel specimens fabricated with EDM demonstrated fatigue strengths reduced by nearly a factor of two, relative to mechanically polished specimens [8]. This study also showed that the reduction in fatigue life could be mitigated by using lower currents in the EDM process. The same authors also presented evidence indicating the fatigue strength degradation caused by EDM processing could be mitigated by depositing TiN coatings on the steel surfaces using physical vapor deposition [9].

Further studies with tool steel (SDK11) were conducted in 2009 with the intent to improve the fatigue life of EDM'd specimens by suppressing the formation of surface cracks through optimization of the electrical parameters employed [10]. Use of higher current and shorter pulse times resulted in surfaces having no microcracks, which displayed longer lifetimes in axial fatigue tests conducted in tension (load ratio, $R = 0.1$).

Fatigue limits of Ti–6Al–4V specimens with ground surfaces and with surfaces "eroded" by EDM were investigated in 2011 using small (10×55 mm) specimens in bending [11]. Although low surface roughness values ($R_a \sim 0.2$ μm) were measured for both types of surfaces, the reported fatigue limits for both classes of specimen were only about 200 MPa. This value is much lower – by a factor of two to three – than fatigue limits measured with conventionally machined specimens as presented in the Military Handbook, cited earlier, and in our own studies presented herein.

The influence of EDM processing on the fatigue strength of Ti–6Al–4V has most recently been examined as part of research striving to enhance adhesion to the surface of medical implants. Using very aggressive EDM process parameters, hour-glass shaped samples were fabricated from bi-modal, annealed $\alpha + \beta$ Ti–6Al–4V, resulting in reported roughness values of $R_a = 11.6$ μm and $R_{max} = 78$ μm [12]. Rotating-beam tests demonstrated severely reduced fatigue strength due to the EDM process: electropolished specimens produced a fatigue limit of approximately 550 MPa, while that of the EDM'd specimens was less than 100 MPa. This degradation was attributed both to a high population of microcracks and the presence of tensile residual stress in the surface of the specimens produced with EDM. In a parallel study, the authors explored the effect of microstructure (equiaxed, bimodal and coarse lamellar) on the fatigue strength of EDM processed specimens [13]. These specimens were reported to have the same roughness as in the prior work, while the electropolished specimens were reported to have "zero roughness." Fatigue tests conducted with electropolished specimens demonstrated equal lives for the equiaxed and bimodal microstructures, and poorer fatigue performance for coarse lamellar material. The fatigue strength of EDM specimens appeared relatively independent of microstructure, and was found to be about a factor of two lower than that of electropolished specimens. The endurance limit of bi-modal, EDM-processed specimens was demonstrated to be only about 100 MPa; stress relieving at 500 °C raised this value to approximately 200 MPa.

Fabrication of metallic components using EDM generally creates residual tensile stresses within the surface layer, because during cooling it shrinks while restrained by the adjacent cooler interior material. This effect is exacerbated by the low thermal conductivity of titanium. Residual stresses in Ti–6Al–4V plate machined with micro-EDM were measured recently using a nanoindentation technique, revealing tensile stresses of up to 350 MPa at depths up to 12 μm [14]. In another study, measurements of residual stress were conducted using a hole-drilling/strain-gage technique, resulting in measured tensile stresses of up to 250 MPa at depths up to approximately 40 μm in titanium-alloy bars having surfaces machined with EDM [15]. Because these levels of measured residual stress are a significant fraction of the fatigue limit, they are likely to contribute directly to a reduction in fatigue strength.

Magnitudes of stress introduced into components processed with EDM can be modulated, to some extent, by machining technique. In a recently published study, residual stresses in EDM-cut tool steel were measured as a function of depth of machining cut. Data reported show that successively finer EDM cuts resulted in reduction of the peak residual stress, from over 500 MPa after the first cut, to about 300 MPa after the fourth finishing cut with EDM [16]. The data also show a reduction in penetration of the residual stress field with each finer finishing cut. By utilizing "low discharge energy and reversed polarity", average surface roughness values of $R_a \sim 0.2$ μm were achieved with EDM cuts in tool steel.

Influential parameters available to the EDM operator include the choice of electrode material, electrical discharge time and current. Research published in 2007 explored the effect of these parameters on the surface roughness and recast-layer thickness in specimens of Ti–6Al–4V cut with wire EDM [17]. It was shown that the average recast-layer thickness could be reduced from nearly 100 μm to about 5 μm by reducing both the pulse duration and current and by using aluminum wire versus graphite or copper. This improvement was accompanied by a corresponding reduction in reported surface roughness, from almost 10 μm to less than 1 μm. Also demonstrated was a reduction of the density of surface microcracks formed, with increasing pulse current and

decreasing pulse duration. Another study focused on adjusting EDM process parameters to reduce surface roughness, achieving $R_a \sim 6$ μm on Ti–6Al–4V [18]. Much smoother surfaces ($R_a \sim 2$ μm) were produced on steel specimens in this study, using similarly optimized parameters; this effect was attributed to the higher thermal conductivity of steel. Substantial improvement in the quality of EDM surfaces has been achieved through the use of "minimum damage generator technology" [19]. With this approach, which varied not only the electrical current but also the pulse waveform and frequency, surfaces with $R_a < 0.5$ μm were achieved with both Inconel 718 and Ti–6Al–4V specimens. Strikingly, these surfaces appeared to have recast layers of negligible thickness. We note here that no reports of the influence of EDM parameters on the fatigue life of titanium alloys have been discovered through our efforts.

It is well-known that surface finish can influence the fatigue life of materials quite strongly. During high-cycle fatigue of many metals, the majority of cyclic lifetime (up to 90%) is consumed during the creation of an initial flaw, or sub-critical crack [20,21]. The presence of microcracks in brittle, thermally-processed surface layers – typical of EDM processing – creates conditions ripe for pre-existing flaws to exist. In such cases, it is to be expected that the lifetime of parts placed into cyclic stress conditions would be abbreviated, relative to nominally similar components absent such defects.

Techniques developed to enhance the fatigue behavior of steel and aluminum have also been applied to titanium. Two principal categories of methods have been explored: those intended to reduce surface defects such as pitting, intergranular voids and microcracks, and those intended to impose a beneficial residual compressive stress near the material surface. Techniques employed to decrease roughness, or mitigate other detrimental surface defects, include mechanical polishing, electro-chemical polishing [22], post-sintering heat treatments [23], coating with titanium nitride by physical vapor deposition [8,24], and plasma coating with hydroxyapatite [25,26]. Treatments to create compressive residual stresses within material surfaces include bead-blasting [27,28] (classically referred to as shot peening), deep rolling [29], grit-blasting [30], laser shock peening [31,32], ultrasonic peening [33], and low-plasticity burnishing [34]. Reports of research investigating the effect of these treatments upon the fatigue life of titanium alloys present results that are somewhat mixed, but the general trend exists for enhancement of fatigue lifetime with reduction in surface roughness and imposition of compressive residual surface stress. Virtually all of these research efforts incorporated conventional machining techniques, rather than EDM.

1.3. Scope of the present work

This study was performed to remedy the outstanding lack of measured fatigue strength for the most ubiquitous titanium alloy (Ti–6Al–4V) with surface conditions produced by state-of-the-art EDM processes. Tensile fatigue tests were conducted using specimens fabricated from a single lot of annealed sheet material, typical for many aerospace components. Reference fatigue behavior was obtained from specimens produced with conventional machining. The effect of different EDM processes was explored by fabricating groups of specimens at three different shops. Using specimens fabricated with the EDM process that produced the greatest surface roughness, the benefit of four post-processing techniques (electrochemical polishing, chemical milling, bead blasting and thermal stress relieving) was explored.

Extensive surface characterization was performed to establish correlation between surface topography resulting from the different fabrication processes and the resultant fatigue behavior. Optical microscopy, laser profilometry, and scanning electron microscopy (SEM) were used to measure surface roughness, recast-layer thickness, microcrack density and intrinsic defect size. The effect of post-processing technique on these parameters was measured and is discussed in relation to corresponding improvements of fatigue strength.

Measured fatigue-strength data are presented in traditional S–N plots. The largest family of specimens was machined conventionally to provide a reference or "baseline". Fatigue data from these specimens are compared to the most appropriate, widely-used data from the MMPDS. Data from the three EDM process are then compared to this baseline. Fatigue strengths from the various post-processed specimens are compared to their unaltered EDM counterparts. Special attention is paid to the fatigue-crack initiation sites, to establish whether the fatigue data from each specimen is indicative of influences from the production processes, or represents intrinsic behavior of the material.

2. Experimental details

2.1. Material description

The material used for this study was Timetal®6–4, purchased in sheet form in the annealed condition (760 °C, 30 min). Reported chemical composition for this material is listed in Table 1. One single lot ("heat") of material was used to produce all specimens, to eliminate possible influences from different batches. The mill certificate reports the 0.2%-offset yield strength as 951 MPa for specimens in the longitudinal orientation, while tests conducted in our own laboratory demonstrated average yield strength of 973 MPa when tested in uniaxial tension at a strain rate of ~0.0001/s. The microstructure of this dual-phase material is bi-modal, as shown in micrographs reproduced in Fig. 1, with isolated lamellar $\alpha + \beta$ colonies interspersed between nearly equiaxed, connected α grains having sizes ranging from approximately 5 to 15 μm.

2.2. Specimen preparation

All fatigue specimens used in this study were conventional tensile "dog-bones", contoured to dimensions consistent with ASTM Standard E466-07 as shown in the drawing in Fig. 2. In the first step, 300-mm square plates of the raw sheet were Blanchard-ground to achieve uniform thickness and flatness. The perimeter of each specimen was then cut using a water-jet process, with the long axis of specimens aligned with the longitudinal (rolling) direction of the sheet. Excess material (~1.5 mm) was retained along the contoured edge so that the finished profile (the "test surface") could be machined using either edge-milling or EDM.

In the next step, the flat faces of all specimens were precision lapped to remove all visible traces of grinding. This process was performed iteratively in conjunction with surface roughness measurements using laser profilometry, to ensure that the roughness of the specimen faces would be lower than that of the machined test surfaces (edges). This important step was taken to reduce the likelihood of fatigue cracks initiating from the flat surfaces, which would result in fatigue data not relevant to the focus of this investigation.

The finished edge contours of one group of (20) specimens were machined conventionally, using the sides of four-fluted, carbide

Table 1
Chemical composition (weight%) of titanium alloy used for fatigue specimens.

Fe	Al	V	C	O	N	Y	H	Ti
0.18	4.0	6.38	0.018	0.18	0.007	<0.0005	25×10^{-6}	Balance

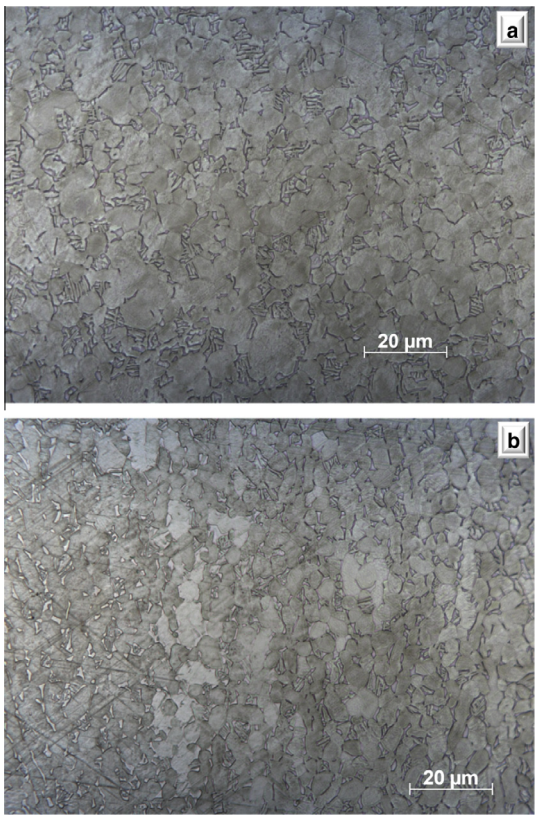

Fig. 1. Microstructure of α + β Ti–6Al–4V used in this study as indicated by optical micrographs (1000×) of longitudinal (a) and transverse (b) etched surfaces.

end mills. Cutting was executed in several stages, each removing sequentially less material. The final pass removed less than 50 μm, resulting in a finish with very fine marks that could barely be detected with the naked eye.

Specimen "blanks" were provided to three independent shops to produce our fatigue specimens using EDM. Each shop was requested to create the "best" surface possible using their own selection of optimized machine parameters. The EDM machines utilized were three to five years old, representing typical modern machines employed by the industry. Specific parameters used by each machine will not be related here, since optimal settings are unique and should be fine-tuned for each machine, material type and thickness. Moreover, it is not the purpose of this study to reveal proprietary techniques, but rather to investigate the impact of modern, "best practice" EDM processes on fatigue strength and possible post-treatments that might improve fatigue behaviors.

Four groups of specimens produced with the EDM process that demonstrated the greatest roughness were subjected to various post-treatments, with the goal of revealing any restorative effect they might have upon fatigue behavior. Specifically, lots of several EDM'd specimens were given the following treatments. Bead blasting of one group of specimens was performed using 50-μm silica beads issued from a 2.4-mm diameter nozzle at 400 kPa pressure, hand-held about 3 cm away from the surface, moving across the length of each contoured edge in about 15 s. Another group was electrochemically polished using a proprietary solution based upon nitric acid, with the instructions to remove a thickness of 10–20 μm from all surfaces. A similar group was also electrochemically polished, but then given a thermal stress-relieving procedure at 594 °C for two hours. A final set of specimens was chemically milled after EDM machining, using a solution incorporating nitric acid, with the similar goal to remove 10–20 μm from all surfaces.

2.3. Specimen surface characterization

To enable correlation of the surface condition resulting from each fabrication process with the resulting fatigue behavior, extensive characterization of specimen surfaces was performed. Optical microscopy of both conventionally milled and EDM surfaces are shown in Fig. 3. Tool marks in the conventionally-machined surface are quite apparent at high (1000×) magnification. The EDM'd surfaces from shops 1 and 2 appear to have similar topography, but the pitting in the EDM surface from shop 3 appears to be deeper, with more pronounced craters and globules.

Electron microscopy of the machined surfaces was more revealing. The conventionally-machined surfaces appeared quite planar, as shown in the SEM image of Fig. 4a, with minute shards of material clinging after having been sheared by the cutting process. All three of the EDM processes generated common features remaining on the surfaces: mounds and fine globules of solidified melt material, re-entrant cavities or holes, and microcracks of various sizes. These cracks were distributed across all EDM surfaces randomly, with densities typified by the micrographs shown in Fig. 4b–d; examination of several specimens from each EDM shop did not reveal distinctions in the density of microcracks. The largest extremes in surface morphology seemed to be evident on the EDM surfaces produced by shop #3.

Surfaces that had been post-processed after EDM were examined with SEM to explore the resulting surface conditions and topography. Dramatic changes were generated through electropolishing, as revealed in the micrographs shown in Fig. 5a and b. These images show a surface devoid of discrete globules, re-entrant crevices and microcracks. In fact, all visible evidence of EDM influences were removed by electropolishing, which transformed the surface into an array of equally dispersed fine nodules, about 150-nm in diameter. Energy-dispersive X-ray spectroscopy (EDS) was performed on these nodules, indicating the presence of elements identical to those in the base metal. Because the penetration depth of the electron beam was greater than the nodule size, and EDS can't readily detect hydrogen, the possibility that the nodules might be hydrides was considered.

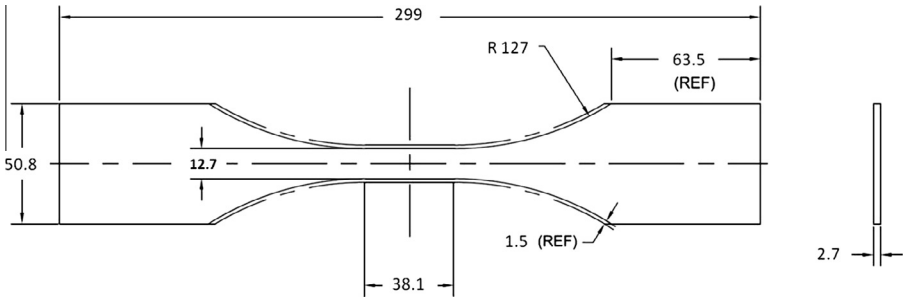

Fig. 2. Geometry and dimensions (mm) of tensile fatigue specimens.

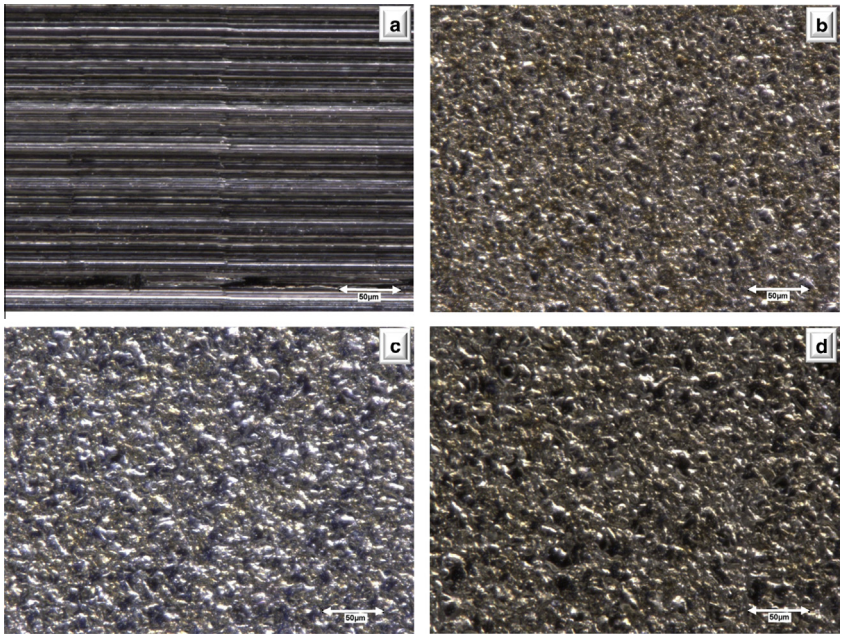

Fig. 3. Optical microscopy (1000×) of specimen test surfaces conventionally machined (a), and EDM processed by shops #1 (b), #2 (c) and #3 (d).

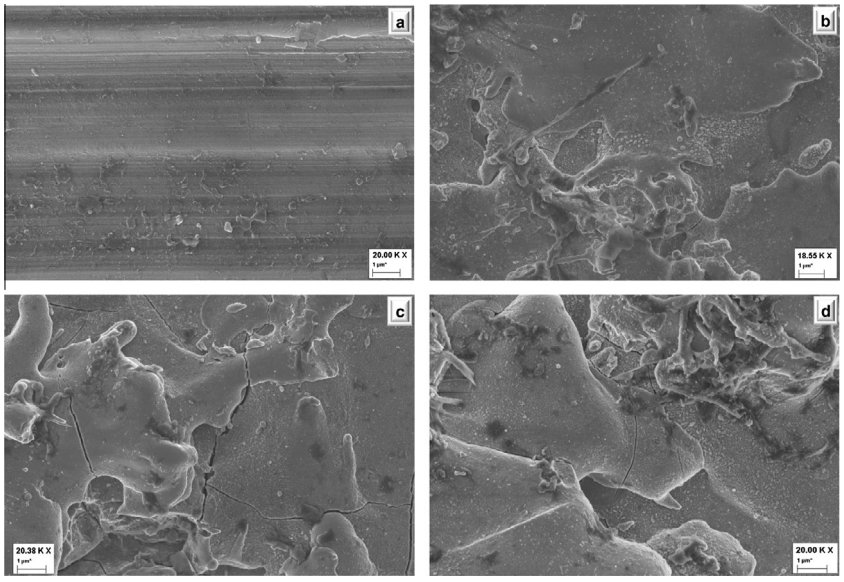

Fig. 4. Scanning electron microscopy (SEM) of specimen test surfaces conventionally machined (a), and EDM processed by shops #1 (b), #2 (c) and #3 (d).

Published images of etched pure titanium show porous-looking, dimpled surfaces with hydrides grown in floral shapes [35–37], while examples of etched Ti–6Al–4V demonstrate ordered nano-dimples with "tunable" features resulting from selective removal of alloying elements [38]. Similarly, it is possible that the chemical process involved in our electropolishing removed one or more alloying elements preferentially, creating the repeated nodular structures present on the entire surface. Though this process could be a topic for further research, it is outside the scope of the present investigation.

The bead-blasted surfaces still retained the large globular mounds, holes and crevices generated within the re-cast layer, as shown in the micrographs reproduced in Fig. 5c and d. Although these suggest that bead-blasting removed only minimal amounts of recast layer, it is apparent that bead-blasting stripped away all lightly-attached features such as fine droplets and tendrils. The images in Fig. 5 also demonstrate that bead-blasting chipped fragments from the surface and promoted further micro-cracking, subdividing the surface into small platelets with sharp, angular features.

Surface roughness of the fatigue specimens was measured using a laser profilometer (Cybertechnologies CT-300) with height resolution of 10 nm. This instrument was chosen instead of a mechanical profilometer, because the physical tips of those instruments are typically hemi-spheres with diameters ranging from 2 to 5 μm. Use of such a tool would permit measuring peak surface heights, but would be inherently limited in ability to detect narrow crevices, or valleys. Because fine crack-like features that might be created by EDM processing present ideal flaws to enable initiation of fatigue cracks, the ability to detect such features was an

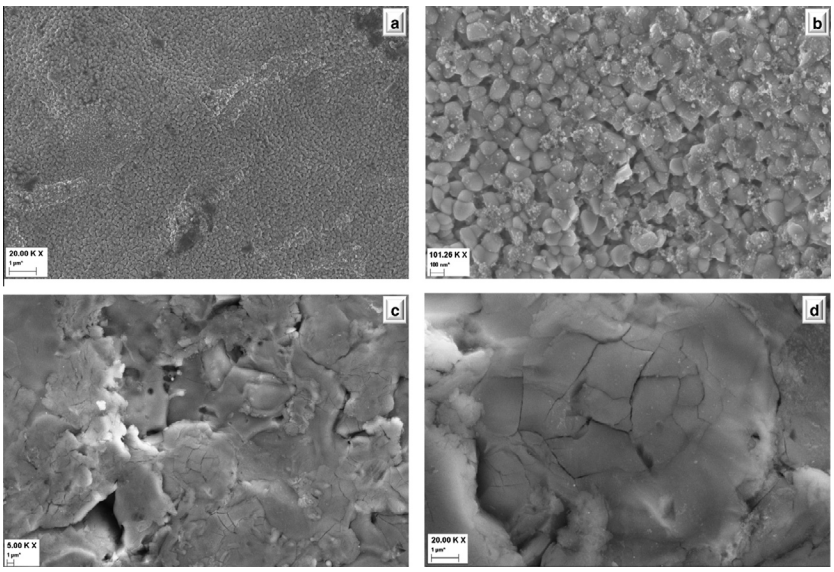

Fig. 5. SEM images of titanium specimen surfaces EDM'd (by shop #3) and postprocessed with electropolishing (a, b) and bead blasting (c, d).

important aspect of our surface roughness measurements. The sensor used on our profilometer has a laser-spot size of 0.9 μm, enabling lateral resolution of approximately 0.5 μm. Three-dimensional images of typical surface profilometry are shown in Fig. 6. As the scale bars imply, the height extremes of the random EDM features are about twice the magnitude of the periodic tool marks created by the conventional machining process.

Surface roughness was measured on both "test surfaces" of three fatigue specimens of each production technique. In addition to the commonly reported average roughness (R_a), we included

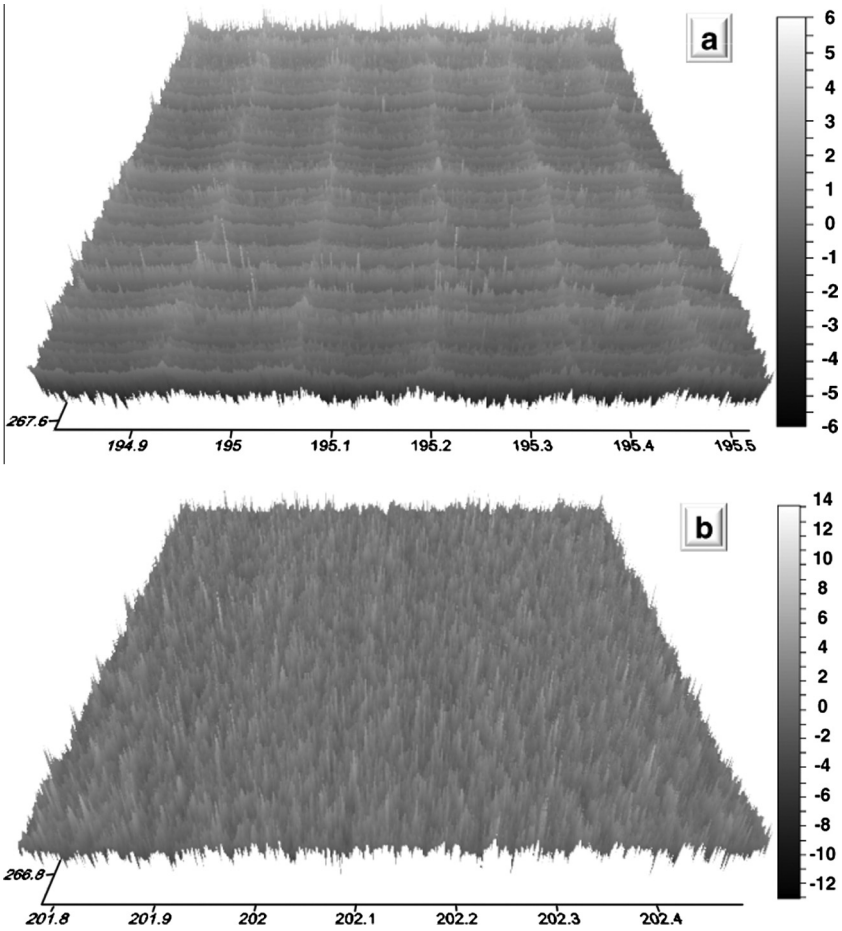

Fig. 6. Three-dimensional representation of laser profilometry of conventionally machined surface (a) and surface EDM'd by shop #3 (b); lateral dimensions in (mm), height in (μm).

measurement of peak-to-valley roughness (R_{p-v}) since that parameter is more indicative of flaws capable of initiating fatigue cracks. Compiled in Table 2 is a summary of these measurements. Although the measured R_a of conventionally-milled surfaces was in the same range as that of the surfaces EDM'd by shops 1 and 2, the peak-to-valley roughness of surfaces EDM'd by shop 1 was substantially greater than that of the conventionally-milled surfaces. The surfaces EDM'd by shop 3 were significantly rougher, by both measures, than all other surfaces. The post-processing techniques were effective in reducing the roughness of the surfaces EDM'd (by shop #3). We note here that the measured R_{p-v} of specimen faces was in the range of 10–20 μm, consistently lower than that of the test edges.

2.4. Fatigue testing procedures

Fatigue testing was conducted in tension mode, with load ratio $R = 0.1$, in an Instron model 8501 servohydraulic machine using a 100-kN load cell. Great care was taken to align the load train of this machine, since misalignment between the machine and specimen axes generates bending stresses which can be of comparable magnitude to the nominal axial stress. Indeed, such misalignment is recognized as an important factor contributing to the wide scatter witnessed in much fatigue data [39]. To facilitate precise alignment of our machine, a fixture enabling adjustment of two translational and two angular degrees of freedom was installed between the cross-head and the load cell. Using one of our fatigue specimens instrumented with twelve strain gages, bending strains were monitored with special-purpose software while the alignment fixture was adjusted. Using this procedure, the bending strains at all locations in the specimen gage length were reduced to less than 1% of the axial strain. This alignment achieved is significantly better than the goal suggested by ASTM E1012, which recommends that the bending strains be reduced to less than 5% of the nominal axial strain [40].

Fatigue specimens were subjected to cyclic loading using a sinusoidal waveform at 10 Hz. The control parameters of the test machine were tuned to ensure that variations in the peak applied load remained less than 0.1% of the prescribed peak load, throughout the loading history. All testing was conducted at room temperature (between 20 and 25 °C). Twenty conventionally-milled specimens were tested, commencing with peak loading of 98% of the material yield strength and progressing with each specimen tested at a lower peak load. Cyclic loading was applied continuously to each specimen until failure occurred or a history of 8 to 10 million cycles had been applied, at which point the testing was halted. For the purposes of this study, those data points were considered "run-outs" and provide an indication of the approximate endurance limit. Each group of EDM'd specimens was tested in a similar manner, except the maximum peak load was limited to about 75% of the yield strength. Those test groups consisted of: 8 specimens from both shop #1 and #2, and 32 specimens from shop #3. This latter group was divided into 8 specimens left unaltered, 10 bead blasted, 10 electropolished and 4 chemically milled.

Table 2
Roughness of fatigue specimen "test" edges, measured with laser profilometer.

Machining method	Treatment	R_{p-v} (μm)	R_a (μm)
Conventional milling	None	15–30	1.1–1.6
Wire EDM; Shop 1	None	23–41	1.1–1.4
Wire EDM; Shop 2	None	22–33	1.1–1.3
Wire EDM; Shop 3	None	55–85	1.8–2.6
Wire EDM; Shop 3	Chemical Mill	32–63	1.3–1.6
Wire EDM; Shop 3	Electropolish	22–55	0.9–1.3
Wire EDM; Shop 3	Bead Blast	22–26	0.9–1.1

3. Results

3.1. Fracture morphology

The fracture surfaces generated by the failure of our fatigue specimens were examined closely to determine the nature of the initiation sites. In cases where the cracks initiated from the machined edge (test surface), the stress/lifetime data are directly relevant to the goals of this study and contribute to the primary results. In cases where fatigue cracks initiated at interior defects, those data provide indications of the intrinsic fatigue behavior of this material. In rare cases where fractures originated on the flat faces, at flaws remaining after the lapping processes, those data present only minimum lifetimes under the applied loading and provide data of little relevance to the effects of machining processes focused upon within this study.

Typical fracture surfaces generated following initiation at the machined edges are shown in Fig. 7, where optical micrographs of two failed specimens show similar growth of the fatigue cracks along planes normal to the applied loading. The chevron shapes were formed when the net section was no longer sufficient to withstand the peak cyclic load, and final failure occurred by a process of ductile rupture forming the slopes with steep angles. Note that the symmetry about the center line in the direction of crack growth indicates the absence of out-of-plane bending.

The vast majority of fatigue specimens in this study formed fracture surfaces with initiation and growth processes typified by those shown in Fig. 7. The nature of fracture initiation sites was usually identified readily through the use of optical or electron

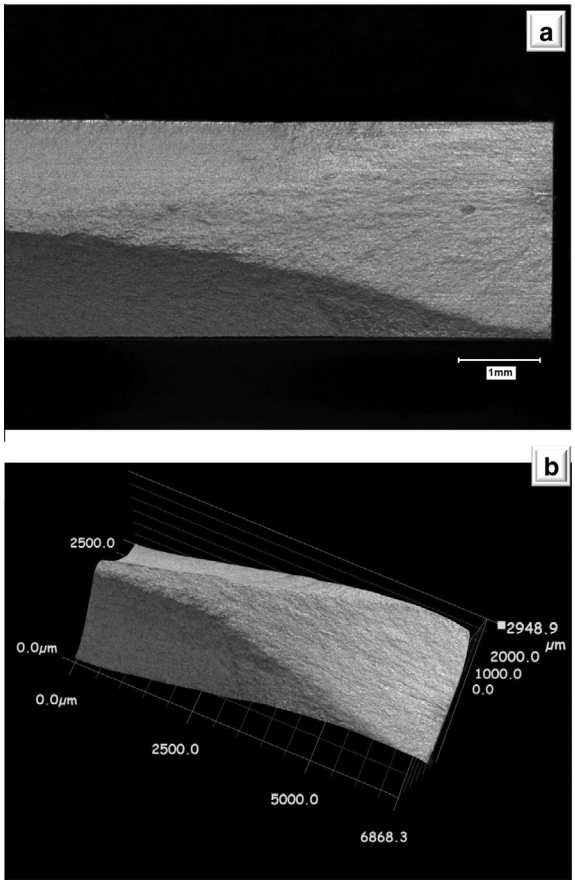

Fig. 7. Optical microscopy (digital, 50×) of fatigued specimens, showing two typical examples of fatigue cracks originating from EDM surface (right edge) and propagating stably in very symmetrical manner.

microscopy. Fatigue fractures in specimens with EDM'd edges initiated invariably at voids present in the recast layer. Shown in Fig. 8a is an example of a fracture origin at a void in recast material, extending through to the base metal. Another initiation site is shown in Fig. 8b, where a void within the recast layer is evident in the fracture surface, but would not have been visible through inspection of the surface prior to fracture, since a thin layer was formed over the void during solidification of the melt material. In this case, the EDM process created further damage and possible voiding at the interface with the parent material below the recast layer. Such flaws clearly present prime sites for initiation of fractures through elevation of the stress concentration (or stress intensity factor).

Fatigue specimens that did not develop well-behaved, edge-initiated fractures either failed through fracture processes originating at the face (Fig. 9a) or within the interior (Fig. 9b). (Note that these fracture surfaces display remarkable symmetry, again demonstrating the lack of bending stresses.) Though a few fractures (8, in total) did originate at specimen faces, only two appeared to be caused by a scratch remaining from the Blanchard-grinding process. Most of the fractures appearing to emanate from the highly lapped, flat surfaces actually originated at voids inherently located just beneath the surface, as illustrated by the micrographs in Fig. 10.

Other examples of intrinsic, interior defects in this alloy that have the potential to give rise to fatigue fractures, if surface initiation is suppressed, are shown in Fig. 11. Irregularly shaped inclusions were noted on many fracture surfaces examined in the electron microscope, with diameters ranging from 5 to 20 μm. Interior voids were observed less frequently, and though very sharply defined, they were much smaller than the inclusions.

3.2. Recast-layer thickness

Measurements of the recast-layer thicknesses produced by the three EDM processes were obtained with scanning electron microscopy (SEM) of the fracture surfaces where they intersected the EDM'd edges. Thorough examinations of three specimens from each EDM shop were conducted; representative examples of images acquired from each are shown in Fig. 12.

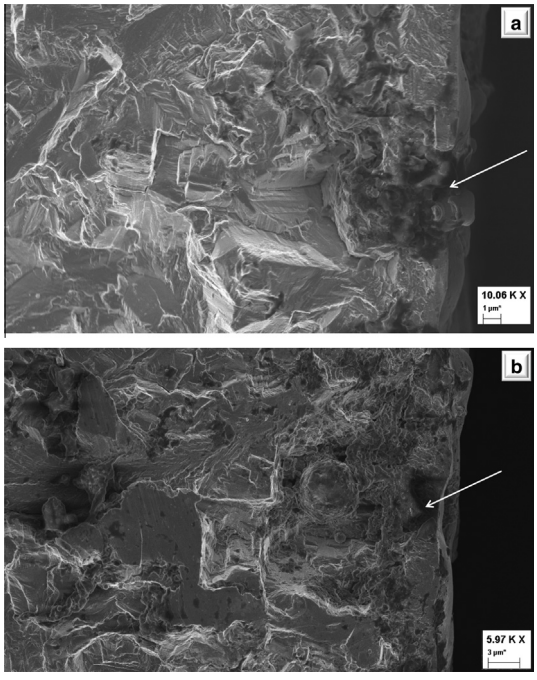

Fig. 8. Examples of EDM-induced damage at fatigue-crack initiation sites. Voids (indicated by arrows) were created through recast layer in (a), within the recast layer and extending below to the interface in (b).

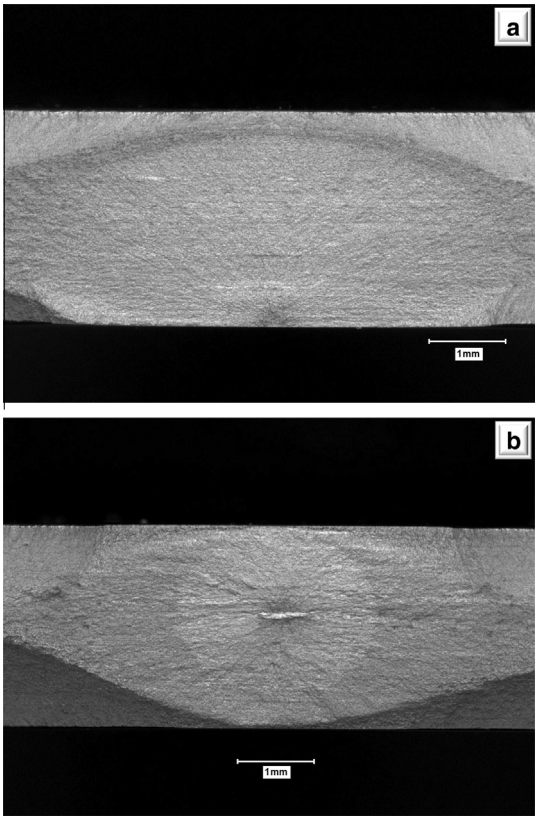

Fig. 9. Fatigue cracks originating at face (a) and within the interior (b).

Recast layers on specimens from shop #1 consistently produced thickness measurements ranging from 2 to 3 μm. The micrographs reproduced in Fig. 12a and b shows these layers to be comprised of somewhat ex-foliated material, split apart into two or more sublayers. Moreover, wherever the recast layer was examined, local regions appeared to be very poorly attached to the parent material or to have partially separated during the fracture process.

Specimens produced by the EDM process at shop #2 demonstrated the thinnest recast layers. While local instances of solidified globules were found to be about 2-μm thick, as shown in Fig. 12c, the thickness of the continuous layers appeared to be slightly less than 1-μm thick. These recast layers were not fragmented nor split apart, and remained well-attached to the base material.

Recast layers on the surfaces produced by shop #3 were consistently at least 1-μm thick, with many sections revealing much thicker (2–3 μm) mounds of solidified material, as shown in Fig. 12d. Partial separation of these recast layers from the parent material was evident at all locations, and they appeared to be formed of two distinctly separate layers. Electropolishing removed these recast layers entirely, and created what appears to be a chemically altered surface layer (see Fig. 5a and b) with a uniform thickness of about 200 nm, as shown in Fig. 13a. This surface layer is intimately attached to the base material, but in some cases partially separated during the fracture process. Bead blasting produced little change in the average thickness of recast layers, but did reduce the height extremes by abrading the mounds and globules. The upper edge of a typical bead-blasted recast layer is shown in Fig. 13b, where delamination is apparent and fragments of broken material are seen to be clinging or partially attached.

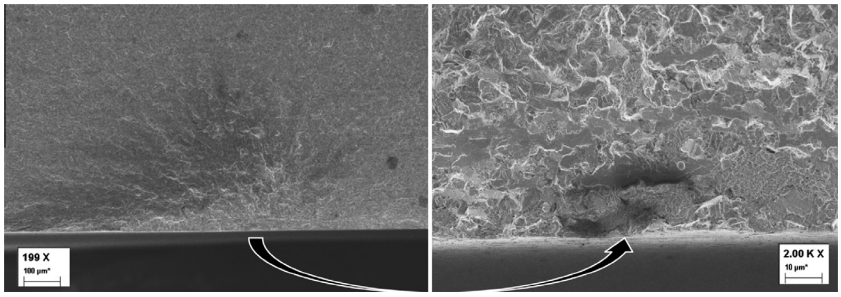

Fig. 10. SEM of fatigue crack apparently originating on specimen face, but actually initiating at subsurface void.

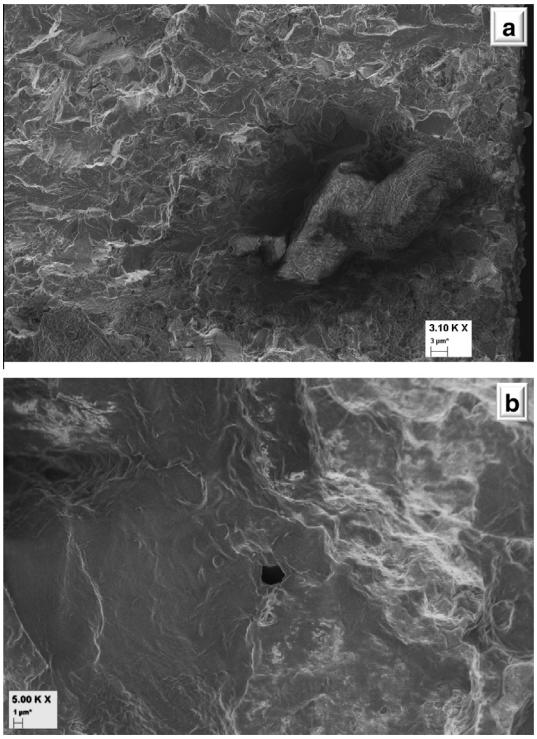

Fig. 11. Examples of intrinsic defects within the Ti–6Al–4V material studied: inclusion (a) and void (b).

3.3. Fatigue-strength measurements

Results from fatigue tests conducted with our conventionally-machined specimens are plotted in Fig. 14, in the form of a traditional S–N, or Wöhler diagram. Included for comparison are data published in MMPDS-01, obtained from similar specimens and testing conditions: both groups used annealed, Ti–6Al–4V rolled sheet material with yield strength of approximately 970 MPa, and specimens subjected to axial fatigue with $R = 0.1$. The most notable difference between the groups is that the MMPDS specimens were of "long transverse" orientation, whereas our specimens were longitudinal. We note that the effect of orientation on fatigue behavior for this material (and test conditions) has been shown to be small, and when normalized by yield strength is not discernable or even separable from scatter in the data [41].

Although good agreement exists between the two groups of fatigue data, the MMPDS data display slightly higher strengths for given lifetimes than those produced by our specimens. This may be a result of the MMPDS specimens being polished with emery paper after machining, whereas specimens in this study were tested in the as-machined condition. Nonetheless, our milled specimens produced less scatter in fatigue behavior, as evidenced by comparison of the curve-fitting correlation coefficients.

Measured fatigue behaviors of specimens produced by EDM processing are plotted in Fig. 15, along with results obtained from our conventionally-milled specimens. The fatigue strengths of EDM'd specimens are clearly inferior to those of the milled specimens, and exhibit an apparent trend of differences between the three shops. Specimens processed by shop 1 consistently demonstrated the lowest fatigue strength, while the highest fatigue strengths were generated by specimens EDM'd at shop 2. The intermediate behavior displayed by specimens EDM'd at shop 3 is represented well by the power-law curve fit indicated in the figure. Comparison of that fit to the power-law fit of the fatigue data from our conventionally-milled specimens shows remarkably similar curves, with nearly identical exponents and an offset in strength. This offset can be interpreted as degradation in fatigue strength that can be characterized in two ways: for a prescribed lifetime of cyclic loading, the fatigue strength of EDM'd specimens was 80% of that of conventionally-milled specimens; alternatively, specimens subjected to a given cyclic peak stress displayed 1.5 orders-of-magnitude shorter lifetimes, when EDM'd by shop 3, compared to specimens milled conventionally.

The effect of post-treatments on the fatigue behaviors of specimens produced by EDM at shop 3 is shown in Fig. 16. All treatments reduced the degradation in fatigue strength induced by EDM, but the greatest and most consistent improvement in strength was produced by bead blasting. Electropolishing also improved the fatigue strength of EDM'd specimens consistently, and to nearly the same extent as bead blasting. When electropolished specimens were exposed to a standard thermal stress-relieving process, however, the resulting lifetimes at high peak stresses were similar to the untreated EDM'd specimens. (The stress-relieved specimens had oxidized surfaces, which may have provided crack-initiating flaws of similar severity to those in the un-modified EDM'd surfaces.) The chemical milling treatment resulted in fatigue-strength behavior similar to that produced by electropolishing.

The locations of the fatigue-fracture initiation sites were determined for all of the specimens tested, and are indicated in Fig. 16 as follows. All of the untreated specimens experienced fractures that initiated at the EDM'd edges; those data points have no notations. Fatigue fractures initiated in many of the post-processed specimens at locations within the interior (denoted by "i") or just beneath the flat faces ("s"). Data from specimens whose fractures initiated at flaws on the flat faces are marked with an "f."

4. Discussion

4.1. Influence of EDM process on fatigue strength

Measured fatigue behaviors of all specimens produced by EDM demonstrated diminished performance relative to specimens fabricated with conventional milling techniques, as shown in Fig. 15.

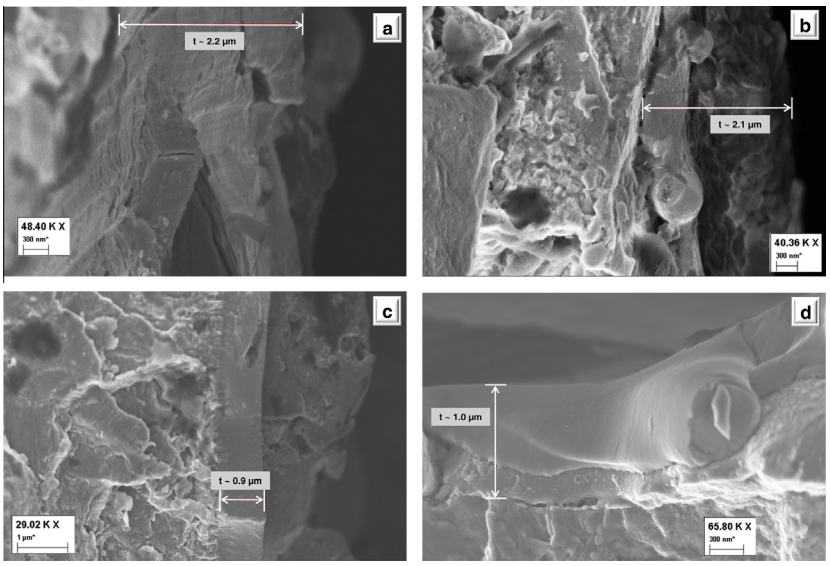

Fig. 12. Measurements of recast-layer thickness on fracture-surface edges: EDM by shop #1 (a, b), shop #2 (c) and shop #3 (d).

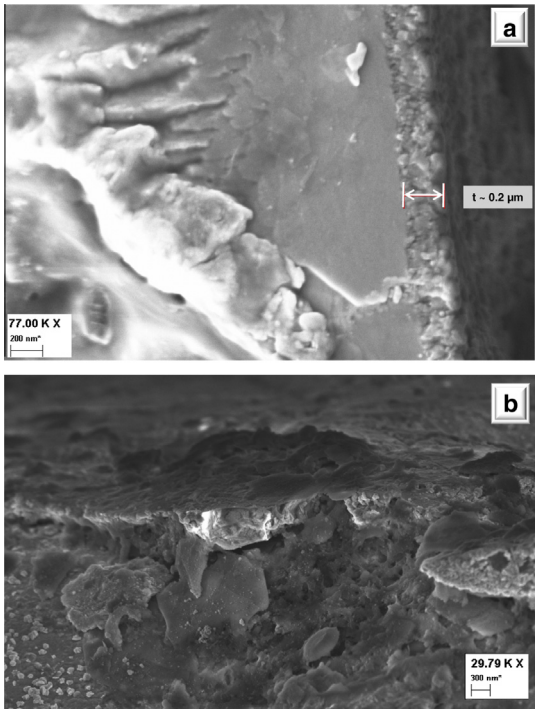

Fig. 13. SEM images of fracture surface near EDM edge, showing surface layers after postprocessing: electropolished (a) and bead-blasted (b).

Using procedures regarded as "best possible" by each of the shops used to source specimens, the most severe reduction in fatigue strength ranged from 20% to 30%, exhibited by specimens EDM'd at shops 1 and 3; the EDM process employed by shop 2 caused less pronounced degradation, evidenced by reduction of fatigue strength by only 10–20% compared to that generated by conventionally milled specimens. Although these reductions in fatigue strength are significantly less severe than strength losses produced by older EDM methods (as related in Section 1.2), even a strength loss of only 20% can erode precious safety margins, presenting design challenges for designers of cyclically-loaded critical components.

Consideration of the fatigue strengths displayed by the three sets of EDM'd specimens raises the question of why one fabrication process produced fatigue behavior superior to the other two. Our microscopy indicated that recast layers on the surfaces produced by all three EDM techniques were populated with similar densities of microcracks, globules and other asperities. Thicker recast layers would, however, enable these crack-like features to be greater in depth and thereby elevate the associated stress intensity factors, thus facilitating initiation of fatigue cracks more readily in thicker layers. Indeed, the EDM process that demonstrated the highest degradation in fatigue strength was executed by shop 1, and those specimens possessed the thickest recast layers, measured consistently from 2 to 3 µm. The EDM process that demonstrated the least detrimental effect upon fatigue behavior was performed by shop 2, whose specimens displayed the thinnest recast layers; our SEM observations of those layers revealed an average thickness slightly less than 1 µm but with occasional bumps as shown in Fig. 12c. Although the recast layers on specimens from shop 3 measured, on average, only slightly thicker than the recast layers on specimens from shop 2, the measured fatigue strengths were significantly lower. The most striking physical evidence that this difference can be attributed to is the greater surface roughness measured on specimens from shop 3, as indicated in Table 2. While the average roughness of specimens produced with EDM by shop 3 ranged from 63% to 100% greater than that of specimens from shop 2, the peak-to-valley roughness measured on specimens from shop 3 was consistently greater by 150%. This observation is consistent with our earlier postulation that fatigue-strength differences are more likely to correlate with R_{p-v} than with R_a.

Although the measurements reported here demonstrate that degradation of fatigue strength of Ti–6Al–4V induced by EDM processing can be significantly lower using modern machines with careful processing than with either older machines (e.g. [2]) or coarser methods (e.g. [12]), it is clear that rewards can be attained by optimizing the operating parameters of each EDM machine for specific materials. All three shops that provided specimens for this study attempted to generate surfaces that would render the best fatigue behavior, but obvious differences resulted. By incorporating results from studies published previously (e.g. [8,10,17–19]) and performing their own trials with EDM electrical parameters, it may be possible to improve the fatigue performance of EDM'd components. In addition, it is also possible to reduce the damaging

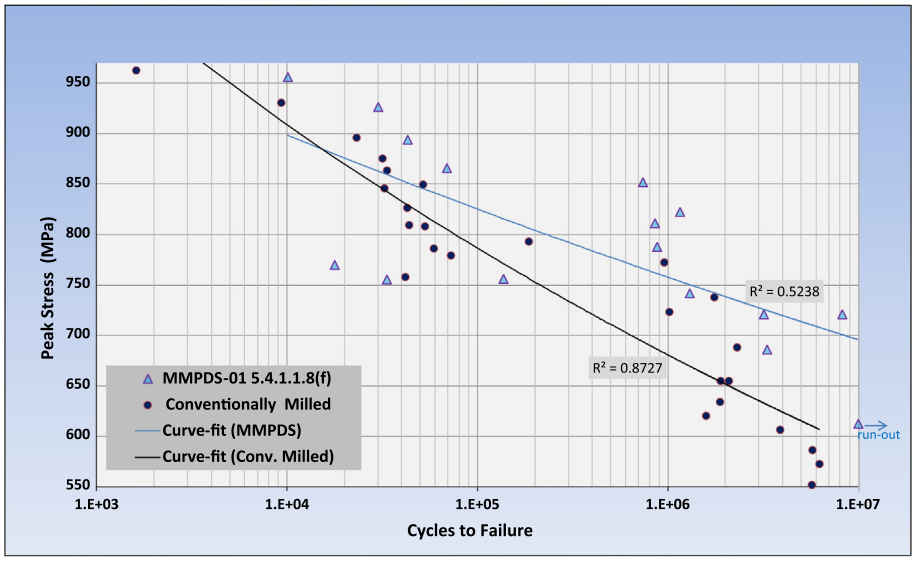

Fig. 14. Measured room-temperature stress–life (S–N) of annealed Ti–6Al–4V sheet, subjected to cyclic tensile fatigue with $R = 0.1$ at a frequency of 10 Hz.

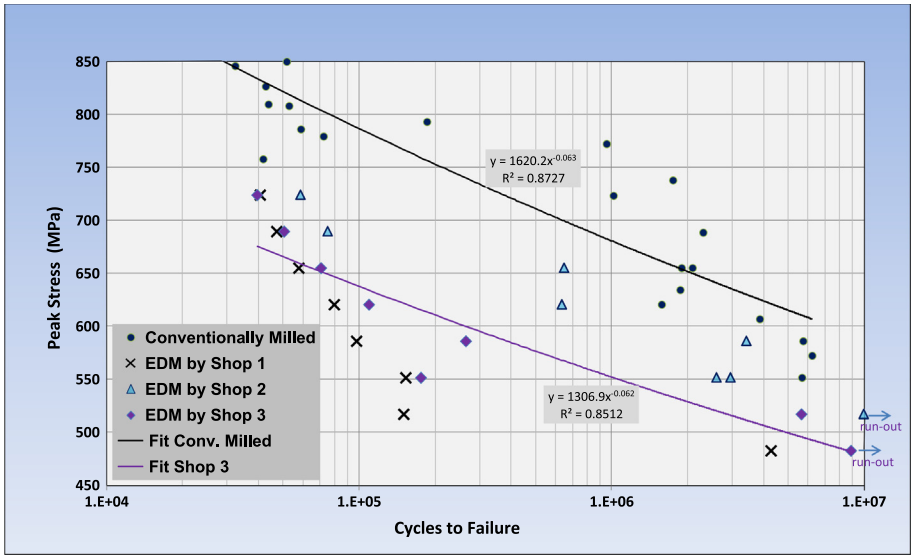

Fig. 15. S–N behavior of annealed Ti–6Al–4V sheet specimens processed with EDM by three different shops versus conventional milling. (Tensile fatigue with $R = 0.1$ at a frequency of 10 Hz.)

influences of EDM by post-processing with an appropriate surface-modifying technique.

4.2. Effects of post-processing

Fatigue behavior of machined metals has been shown to be enhanced by each of several post-processing techniques, including mechanical polishing [8], electropolishing [12], chemical milling [7], beadblasting (shotpeening) [28] and laser peening [29]. Many specimen geometries do not permit some of these techniques, and special circumstances may also limit post-processing options. Moreover, there appear to have been no studies published on the effects of these treatments on the fatigue behavior of T–6Al–4V processed with modern EDM techniques.

The data presented in Fig. 16 show enhancement of fatigue strength resulting from all of the treatments applied to specimens fabricated with EDM, with the exception of thermal stress relieving. This is likely a demonstration that thermal treatments should be performed in an inert, oxygen-free environment to prevent stress-concentrating defects from forming due to oxidation.

Fatigue strengths exhibited by bead-blasted specimens were superior to those of specimens subjected to all other treatments. This may be somewhat surprising, in view of the minimal visible influence bead blasting had (cf. Fig. 5b), but this treatment did reduce measured surface roughness to levels comparable to those of electropolished specimens. The most influential effect that bead-blasting had, however, was to create compressive residual stress within the EDM'd surfaces.

Residual-stress measurements were performed on our specimens by an independent laboratory using a standard, multi-angle X-ray diffraction technique [42]. The method used determined the maximum residual stress in the longitudinal direction (parallel to the fatigue loading axis) beneath the surface, probing the material to the maximum penetration depth of approximately 100 μm. Untreated EDM surfaces showed the presence of modest levels of residual stress (from −30 to +30 MPa). Similar measurements of

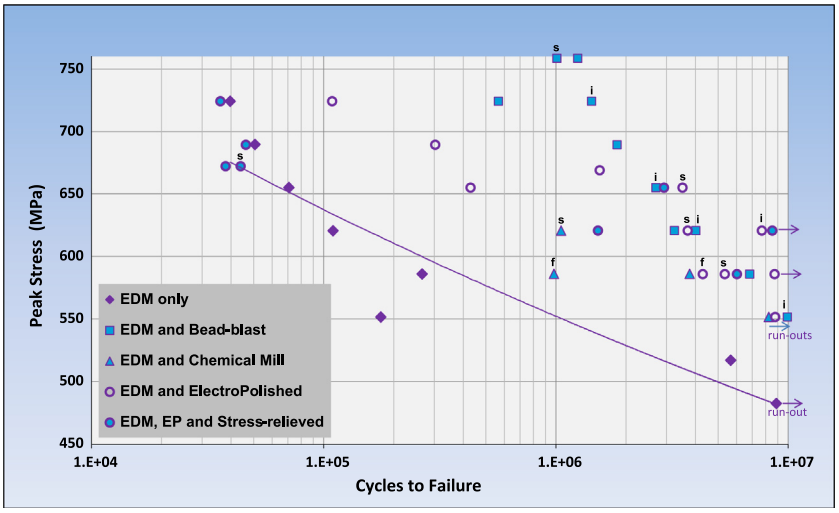

Fig. 16. S–N behavior of annealed Ti–6Al–4V specimens fabricated with the same EDM process (shop 3) and subjected to post-treatments as indicated. (Tensile fatigue with $R = 0.1$, $f = 10$ Hz.)

EDM'd specimens treated with bead-blasting indicated residual stresses of −660 ± 60 MPa in the near-surface region. The effect of this compressive stress upon fatigue strength is manifest in Fig. 16. Electropolishing appeared to have little effect upon surface residual stress in EDM'd specimens, even though this processing resulted in improved fatigue behavior; measured stresses on the edges of those specimens ranged from −30 to +16 MPa. Chemical milling, though similar to electropolishing, resulted in creation of tensile residual stress of approximately 50 MPa.

Many components with intricate geometries or small size do not permit full coverage of post-processing techniques that require physical contact. In particular, small slots and holes that EDM processing is well-suited for are typically not accessible to polishing tools or bead-blasting, yet these very features are prominent stress-raisers that make cyclically-loaded components susceptible to fatigue failures. The beneficial effect of electropolishing on fatigue strength as shown by our data in Fig. 16 is therefore of great practical consequence. The shift in the nature of fracture-initiation sites, from the EDM'd edges in untreated specimens to interior or sub-surface locations, demonstrates that electropolishing removes the deleterious effects of EDM processing to the extent that the intrinsic fatigue behavior of the material is displayed. Chemical milling showed nearly the same effects, although the sample population was low in this study.

5. Conclusions

Baseline fatigue strengths were established for annealed Ti–6Al–4V sheet material tested in tension at $R = 0.1$, using specimens milled with conventional techniques. Due in part to precision alignment of the test machine, these data exhibit less scatter than similar data published in the Military Handbook 5 (now MMPDS). Measured fatigue strength of specimens fabricated using three different, state-of-the-art EDM processes demonstrated a reduction of fatigue strength by 15–30%, relative to the strength of specimens machined conventionally. This strength degradation is attributed to the presence of stress-concentrating defects within the EDM recast layers, examples of which are shown in SEM micrographs. The differences between fatigue strengths displayed by specimens produced by the three different EDM processes were shown to correlate directly to the thickness (1–3 μm) and roughness (R_{p-v} from 22 to 85 μm) of the recast layers. Using specimens fabricated with the EDM process shown to create the roughest surface, post-processing with either electrochemical polishing or bead blasting was demonstrated to alleviate the deleterious effects of EDM, thereby restoring the intrinsic fatigue behavior as indicated by crack initiation at interior locations. The data presented establish that modern EDM techniques are capable of processing Ti–6Al–4V with only modest degradation of fatigue strength, in contrast to data in the literature from outdated EDM machines.

Acknowledgement

This work is sponsored by the Department of the Air Force under the United States Air Force contract number FA8721-05-C-0002. The opinions, interpretations, recommendations and conclusions are those of the author and are not necessarily endorsed by the United States Government.

References

[1] Peters M, Hemptenmacher J, Kumpfert J, Leyens C. Structure and properties of titanium and titanium alloys. In: Leyens, Peters, editors. Titanium and titanium alloys. Wiley-VCH, Federal Republic of Germany; 2003. p. 22.
[2] Donachie MJ. Titanium, A technical guide. Metals Park (Ohio): ASM International; 1988. p. 85.
[3] Kahles JJ, Field M, Eylon D, Froes FH. Machining of titanium alloys. J Metals 1985;37(4):25–35.
[4] Battelle Columbus. Metallic materials and elements for aerospace vehicle structures (MIL-HDBK-5H). U.S. Department of, Defense; 2003: 5–67–73.
[5] Golden PJ, Reji J, Porter III WJ. Investigation of variability in fatigue crack nucleation and propagation in alpha+beta Ti–6Al–4V. Procedia Eng 2010;2:1839–47.
[6] Jha SK, Szczepanski CJ, Golden PJ, Porter III WJ, Reji J. Characterization of fatigue crack-initiation facets in relation to lifetime variability in Ti–6Al–4V. Int J Fatigue 2012;42:248–57.
[7] Military handbook on titanium and titanium alloys (MIL-HDBK-697A); 1974. p. 44.
[8] Guu YH, Hosheng H. High cycle fatigue of electrical-discharge machined AISI D2 tool steel. Int J Mater Prod Technol 2001;16(6/7):642–57.
[9] Guu YH, Hosheng H. Improvement of fatigue life of electrical discharge machined AISI D2 tool steel by TiN coating. Mater Sci Eng A 2001;318:155–62.
[10] Tai TY, Lu SJ. Improving the fatigue life of electro-discharge-machined SDK11 tool steel via the suppression of surface cracks. Int J Fatigue 2009;31:433–8.
[11] Klocke F, Welling D, Dieckmann J. Comparison of grinding and Wire EDM concerning fatigue strength and surface integrity of machined Ti6Al4V components. Procedia Eng 2011;19:184–9.
[12] Janeček M, Nový F, Stráský J, Harcuba P, Wagner L. Fatigue endurance of Ti–6Al–4V alloy with electro-eroded surface for improved bone in-growth. J Mech Behav Biomed Mater 2011;4:417–22.
[13] Stráský J, Janeček M, Harcuba P, Bukovina M, Wagner L. The effect of microstructure on fatigue performance ofTi–6Al–4V alloy after EDM surface treatment for application in orthopaedics. J Mech Behav Biomed Mater 2011;4:1955–62.

[14] Murali MS, Yeo S-H. Process simulation and residual stress estimation of micro-electrodischarge machining using finite element method. Jpn J Appl Phys 2005;44(7A):5254–63.
[15] Stefanescu D, Truman CE, Smith DJ, Whitehead PS. Improvements in residual stress measurement by the incremental centre hole drilling technique. Exp Mech 2006;46:417–27.
[16] Bleys P, Kruth J-P, Lauwers B, Schacht B, Balasubramanian V, Froyen L, et al. Surface and sub-surface quality of steel after EDM. Adv Eng Mater 2006;8(1–2):15–25.
[17] Hasçalık A, Çaydaş U. Electrical discharge machining of titanium alloy (Ti–6Al–4V). Appl Surf Sci 2007;253:9007–16.
[18] Yu J, Xiao P, Liao Y, Cheng M. Surface integrity in electrical discharge machining of Ti–6Al–4V. Adv Mater Res 2009;76–8:613–7.
[19] Aspinwall DK, Soo SL, Berrisford AE, Walder G. Workpiece surface roughness and integrity after WEDM of Ti–6Al–4V and Inconel 718 using minimum damage generator technology. CIRP Annal – Manuf Technol 2008;57:187–90.
[20] Nicholas T. High cycle fatigue. Oxford: Elsevier; 2006. 162.
[21] Newman JCJ, Philips EP, Swain MH, Everett Jr RA. Fatigue mechanics: an assessment of a unified approach to life prediction. ASTM STP 1992;1122:5–27.
[22] Solutions to metal surface problems. Able Electropolishing. Chicago, IL; 2008.
[23] Cook SD, Renz EA, Haddad RJ. Post-sintering heat treatments for porus coated Ti–6Al–4V alloy. Biomat. Med. Dev. Art. Org. 1985;13(1&2):37–50.
[24] Costa MYP, Cioffi MOH, Venditti MLR, Voorwald HJC. Fatigue fracture behavior of Ti–6Al–4V PVD coated. Procedia Eng 2001;2:155–62.
[25] Evans SL, Gregson PJ. The effect of a plasma-sprayed hydroxyapatite coating on the fatigue properties of Ti–6Al–4V. Mater Lett 1993;16:270–4.
[26] Lynn AK, DuQuesnay DL. Hydroxyapatite-coated Ti–6Al–4V Part 1: the effect of coating thickness on mechanical fatigue behavior. Biomaterials 2002;23:1937–46.
[27] Koster WP, Gatto LR, Cammett JT. Influence of shot peening on surface integrity of some machined aerospace materials. The Shot Peener 1970;14(1):34–6.
[28] Wagner L, Kocan M, Ludian T. Fatigue response of the various titanium alloy classes to shot peening. Metal Finish News 2004:5.
[29] Nalla RK, Altenberger I, Noster U, Liu GY, Scholtes B, Ritchie RO. On the influence of mechanical surface treatments – deep rolling and laser shock peening – on the fatigue behavior of Ti–6Al–4V at ambient and elevated temperatures. Mater Sci Eng A 2003;355(1):216–30.
[30] Eberhardt AW, Kim BS, Rigney ED, Kutner GL, Harte CH. Effects of precoating surface treatments on fatigue of Ti–6Al–4V. J Appl Biomater 1995;6:171–4.
[31] Clauer AH. Laser shock peening for fatigue resistance. In: Gregory, Rack, Eylon, editors. Surface performance of titanium. Warrendale (PA): TMS; 1996. p. 217–230.
[32] Ruschau JJ, John R, Thompson SR, Nicholas T. Fatigue crack nucleation and growth rate behavior of laser shock peened titanium. Int J Fatigue 1999;21:S199–209.
[33] Mordyuk BN, Prokopenko GI. Fatigue life improvement of α-titanium by novel ultrasonically assisted technique. Mater Sci Eng A 2006;437:396–405.
[34] Jayaraman N, Prevěy PS, Ravindranath R. Improved damage tolerance of Ti–6Al–4V aero engine blades and vanes using residual compression by design. Granada (Spain): NATO RSV; 2005.
[35] Szmukler-Moncler S, Bischof M, Nedir R, Ermrich M. Titanium hydride and hydrogen concentration in acid-etched commercially pure titanium and titanium alloy implants: a comparative analysis of five implant systems. Clin Oral Implant Res 2010;21(9):944–50.
[36] Frank MJ, Walter MS, Bucko MM, Pamula E, Lyngstadaas SP, Haugen HJ. Polarization of modified titanium and titanium–zirconium creates nano-structures while hydride formation is modulated. Appl Surf Sci 2013;282:7–16.
[37] Conforto E, Caillard D, Aronsson B-O, Descouts P. Crystallograpic properties and mechanical behavior of titanium hydride layers grown on titanium implants. Phil Mag 2004;84(7):631–45.
[38] Wang Y, Singh S, Kruse P. Ordered nano-scale dimple pattern formation on a titanium alloy (Ti–6Al–4V). AIP Adv 2012:2. 032101-1-12.
[39] MTS Service Note. #100-161-434a Variability. MTS Systems Corp., Eden Prairie, MN; 2012.
[40] ASTM Standard E1012. Standard practice for verification of testing frame and specimen alignment under tensile and compressive axial force application. ASTM Internatioinal, West Conshohocken, PA; 2012.
[41] Srivatsana TS, Bathini U, Patnaik A, Quick T. A study of cyclic fatigue, damage initiation, damage propagation, and fracture of welded titanium alloy plate. Mater Sci Eng A 2010;527:6649–59.
[42] Measurements of stress by X-ray diffraction. TEC Materials Testing Division, White paper, Knoxville, TN; 2002.